Article

Geochemical Characteristics of Water Produced from Coalbed Methane Wells in the Southern Qinshui Basin and Construction of an Associated Model: Implications for Coalbed Methane Co-Production

Jie Wu [1,2,3,*], Chen Guo [4,5], Shuxun Sang [1,6,7] and Guofu Li [2,3]

1 School of Resource and Earth Sciences, China University of Mining and Technology, Xuzhou 221116, China
2 State Key Laboratory of Coal and Coalbed Methane Co-Mining, Jincheng 048012, China
3 Jinneng Holding Equipment Manufacturing Group Co., Ltd., Jincheng 048012, China
4 College of Geology and Environment, Xi'an University of Science and Technology, Xi'an 710054, China
5 Shaanxi Provincial Key Laboratory of Geological Support for Coal Green Exploitation, Xi'an 710054, China
6 Low Carbon Energy Institute, China University of Mining and Technology, Xuzhou 221008, China
7 Key Laboratory of Coalbed Methane Resources and Reservoir Formation Process of the Ministry of Education, China University of Mining and Technology, Xuzhou 221008, China
* Correspondence: 15235606904@163.com; Tel.: +86-15235606904

Abstract: The geochemical characteristics of water produced from coalbed methane (CBM) wells contain rich information about the associated geology, environment, and production. This study was conducted in the Southern Qinshui Basin, where produced water samples were collected from 10 typical CBM wells and their ionic compositions and water quality parameters were tested. The differences in the chemical characteristics of the produced water between different producing coal seams and between single-seam production wells (SPWs) and multi-seam co-production wells (MCWs) were compared, and the geochemical formation process of the produced water was revealed. The following conclusions were obtained: (1) the water produced samples that were mainly Na-HCO$_3$-type and were generally weakly alkaline and moderately mineralized. The water produced from No. 15 coal seam was more enriched in SO$_4$, Ca, and Mg compared to that of No. 3 coal seam, and the variations were more intense, reflecting a more complex water chemistry formation. (2) The ionic data of the water produced from MCWs do not lie between the coal seams of SPWs, nor do they satisfy the linear relationship between the ionic compositions of SPWs, reflecting the differences in the water sources between MCWs and SPWs. Water from MCWs tends to communicate with active water sources outside the coal seams, and the produced water contains small amounts of Cl and total dissolved solids, thus inhibiting the pressure reduction efficiency and limiting the effect of CBM co-production. (3) Based on a principal component analysis of the ionic compositions, two characteristic components were extracted, and these represented two types of hydrochemical formation processes. The first type is pyrite oxidation and carbonate dissolution, and its opposite represents sulfate reduction. The second type reflects the groundwater retention and confinement characteristics, and its opposite represents active groundwater or stronger recharge conditions. (4) A geochemical formation model of the water produced from CBM wells in the study area was constructed. Cation exchange adsorption and sulfate reduction were found to be the main water–rock interactions in the coal measure, and they determine the overall water quality of the produced water. Recharge has a relatively significant influence on water produced from MCWs. Pyrite oxidation exists in the water produced from No. 15 coal seam of the Taiyuan Formation, and the higher sulfur content in the coal contributes to this reaction. The results of the study will assist in deepening our understanding of the geochemical formation mechanisms of water produced from CBM wells, and they provide the main reasons for the poor CBM co-production effect from the Shanxi and Taiyuan Formations.

Keywords: produced water; ionic composition; co-production; groundwater chemistry; water–rock interaction

1. Introduction

The geochemical characteristics of the water produced from coalbed methane (CBM) wells provide rich geological, environmental, and production information, and they are important for researching the formation and evolution of CBM, the coal seam water, and the CBM enrichment mechanism and production dynamics, in addition to identifying any hydrodynamic field disturbances caused by CBM production and assisting in determining appropriate produced water treatment processes [1–6]. Previous research conducted on water produced from CBM wells has focused on the ionic composition, stable isotopes, trace elements, and rare earth elements in the water, and the results have effectively guided the identification of gas and water production sources in CBM wells and assisted in predicting the CBM production capacity and conducting environmental evaluations [7–14]. Multi-seam CBM co-production is necessary to improve the efficiency of CBM development in multi-seam areas [15]. However, for CBM co-production wells, the span of the producing interval is large and the drainage relates to different water-bearing units; this forms interlayer interference between the aquifer and coal seam, reduces the drainage and pressure reduction efficiency, and induces an unfortunate situation where high amounts of water are produced but small amounts of gas [16–21]. Conducting geochemical testing and a comparative analysis of the water produced from single-seam production wells (SPWs) and multi-seam co-production wells (MCWs) can provide information that enables identification of the produced water source and the degree of interlayer interference, and this can further help to optimize the co-production program and rationalize the selection of production layers and zones.

The southern Qinshui Basin in North China is a model area for CBM exploration and development in China, and it was the first to achieve commercial CBM development in China. The current production well types in this area include horizontal wells and vertical wells; in this respect, horizontal wells are mainly used for single-seam production and vertical wells are mostly used for multi-seam co-production. The effect of CBM development in this area is variable, and the geological controlling factors of CBM production require further investigation, especially those relating to interlayer interference and the main factors controlling the multi-seam co-production capacity. Therefore, in this study, 10 typical CBM wells in the region were selected, and produced water samples were collected to conduct ionic composition and water quality parameter analyses. The differences in the chemical compositions of produced water between different producing coal seams and between SPWs and MCWs were explored, the mechanisms involved in water chemistry formation and an associated geological model was analyzed, and the significance of the water produced on CBM exploration and development was discussed. The research results are expected to provide a reference basis for further cost reductions and enhancing the efficiency of CBM development in the area, and for promoting the effective development of the abundant CBM resources in the Taiyuan Formation and the efficient co-production of CBM from the Shanxi and Taiyuan Formations.

2. Study Area

The Qinshui Basin is a weakly extruded extensional basin developed on the base of the Paleozoic North China Craton; structurally, it is a large and gentle compound syncline lying in a north-northeast direction with the axis located roughly within the Qinshui–Qinxian–Yushe Districts [22]. The basin is bounded by the Wutaishan uplift in the north, the Zhongtiao uplift in the south, the Huoshan uplift in the west, and the Jinhuo Fault zone in the east [23]. The periphery of the Qinshui Basin is uplifted, exposing the Permian and Triassic strata. The strata in the two limbs of the basin are symmetrical, and the dip angle gradually decreases toward the interior of the basin [24]. The southern Qinshui Basin is generally monoclinic with a northwestern slope, where the tectonics of the eastern and western edges are relatively complex. The development of the Jinhuo Fault zone on the eastern boundary has an important controlling role on the regional tectonics and the evolution of the coal seam, while the Sitou Fault in the center is a closed fault that has an

important influence on the accumulation of CBM in the area [25]. Bounded by the Sitou Fault, secondary folds with axial SN-trending and NNE-trending are mainly developed in the east and west, respectively. The overall structure of the southern Qinshui Basin is relatively simple and the continuity of the coal seam is good, thus providing favorable conditions for coal and CBM development [26].

　　　　The coal-bearing strata in the study area are the Taiyuan and Shanxi Formations in the Carboniferous–Permian; they comprise more than 10 coal seams and have a total thickness of 3.65–23.8 m (Figure 1). The Taiyuan Formation contains 7–9 coal seams, and 1–2 coal seams are mineable (including No. 9 coal seam and No. 15 coal seam), and the Shanxi Formation contains 3–4 coal seams, only one of which is mineable (No. 3 coal seam). Of the seams in the two formations, Nos. 3 and 15 have large thicknesses and stable distributions, and these are the main target layers for CBM exploration and development in this area [24]. Bright coal and semi-bright coal are developed in this area, and the coal seams are dominated by a primary coal structure and a relatively complete coal body structure. Natural fissures are developed, and the fissure types include endogenous fissures, gas expansion, and tectonic fissures, which help to increase the coal seam permeability. The coal seam is highly metamorphosed, which is associated with regional magmatic rock intrusion, and $R_{o,max}$ values are generally above 3% and belong to anthracite [24]. The macerals are mainly vitrinite, followed by inertinite, and the content of exinite is extremely low. Further, No. 3 and No. 15 coal seams have average vitrinite, inertinite, and exinite values of 76.2% and 82%, 18.9%, and 17.6%, and 0.7% and 0.4%, respectively, which relate to low–medium ash coals. The sulfur content of No. 15 coal is significantly higher than that of No. 3 coal seam. The total sulfur of No. 3 coal seam is between 0.21% and 0.50%, with an average of 0.36%, which is associated with ultra-low sulfur coal, whereas the total sulfur content of No. 15 coal seam is 1.84–9.19%, with an average of 3.12%, which is associated with medium–high sulfur coal. Sulfide sulfur is the main sulfur form in No. 15 coal seam, and pyrite constitutes the main carrier of sulfur. The permeability of the coal seams obtained from well tests in this area is mainly less than 1 mD, but that of No. 3 coal seam (average 0.60 mD) is generally higher than that of No. 15 coal seam (average 0.49 mD).
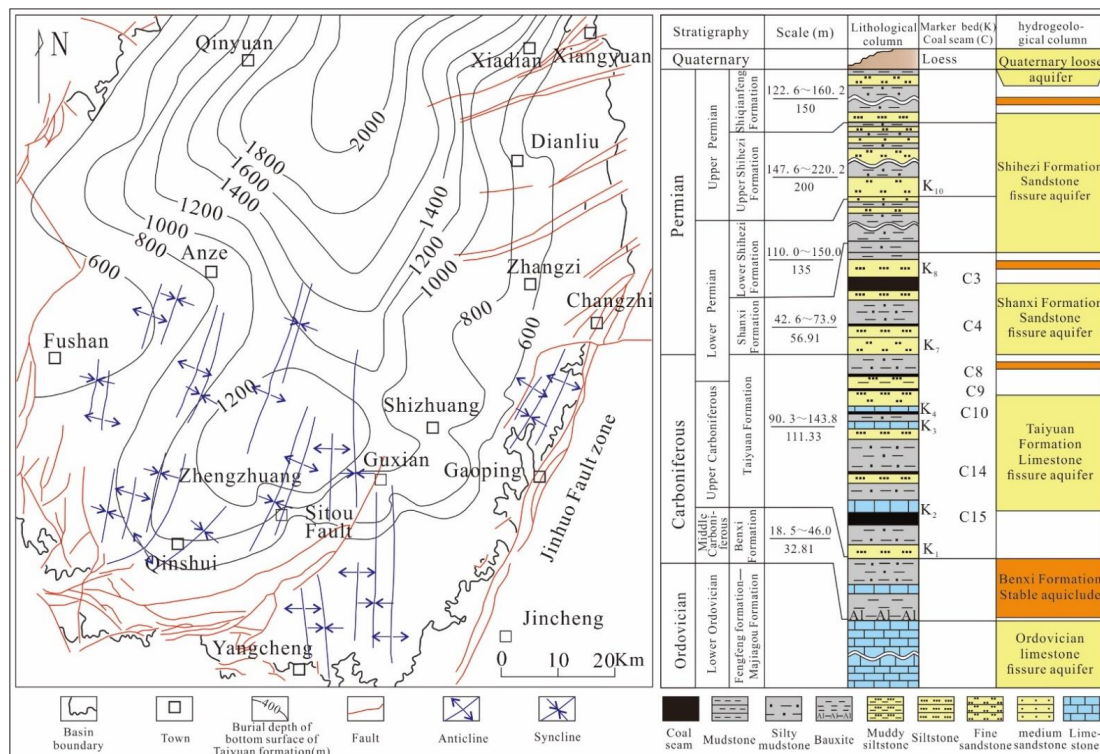

Figure 1. Tectonic map and stratigraphic column of the coal-bearing strata of the southern Qinshui Basin.

3. Sample Collection and Tests

Ten CBM wells in the Panhe block of the southern Qinshui Basin were selected to collect produced water samples in August 2022. The CBM wells had been continuously drained for more than two years. Of the collected produced water samples, two samples were from the SPWs of No. 3 coal seam (labeled 1–2); one was obtained from the SPW of No. 9 coal seam (labeled 3); four were obtained from the SPWs of No. 15 coal seam (labeled 4–7); one was obtained from the MCW of the Nos. 3, 9, and 15 coal seams (labeled 8); and two were obtained from the MCWs of the Nos. 9 and 15 coal seams (labeled 9–10). The sample numbers corresponded to the CBM well numbers (for example, Sample No. 1 was collected from Well No. 1). The water samples were taken directly from the wellhead of each CBM well. Before sample collection, the sampling bottle was flushed with produced water more than three times. The water filled the entire sampling bottle to minimize the influence of air on the water sample. The samples were preserved at an ambient temperature and pressure in a light-free environment, and their ionic compositions and water quality parameters were subsequently analyzed at the State Key Laboratory of Environmental Geochemistry, Chinese Academy of Sciences, Guiyang, China. The ions tested included HCO_3, CO_3, F, Cl, NO_3, SO_4, Na, K, Ca, and Mg. HCO_3 and CO_3 were measured using acid titration, the remaining anions were measured using ion chromatography, and the cations were measured by inductively coupled plasma–atomic emission spectroscopy (ICP–AES). The parameters of pH, total dissolved solids (TDS), and electrical conductivity (EC) were also measured using a portable multifunction water tester (Ispring Water Systems, LLC, Atlanta, GA, USA) during sample collection.

4. Results and Discussion

4.1. Overall Quality of the Produced Water

The ionic compositions and water quality parameters of the produced water samples from the CBM wells are shown in Table 1. The produced water samples were generally weakly alkaline with medium salinity. The anions were dominated by HCO_3, and the ionic concentrations from high to low were $HCO_3 > Cl > SO_4 > F$. Cations were dominated by Na, and the concentrations from high to low were $Na > K > Ca > Mg$. The water sample types were mainly $Na-HCO_3$ type. CO_3 was below the detection limit in all samples.

Table 1. Ionic compositions and parameters of produced water samples.

Samples	HCO_3^- (mg/L)	SO_4^{2-} (mg/L)	Cl^- (mg/L)	F^- (mg/L)	Ca^{2+} (mg/L)	Mg^{2+} (mg/L)	Na^+ (mg/L)	K^+ (mg/L)	Sr^{2+} (mg/L)	TDS (mg/L)	pH	EC (μS/cm)
1	1487.01	0.233	114.053	7.557	3.82	0.44	535.39	4.76	0.27	1076	8.15	2042
2	1447.88	2.741	367.007	5.098	5.34	1.52	633.08	35.84	0.56	1388	8.17	2570
3	1535.92	18.081	123.629	7.289	4.43	1.58	559.63	9.80	0.49	1119	8.27	1990
4	1379.40	7.713	397.285	8.664	6.75	5.53	622.36	66.97	0.60	1446	8.19	2630
5	880.47	635.349	239.218	4.668	69.90	31.63	549.88	12.33	2.61	1474	7.61	2690
6	1467.44	5.498	194.653	10.243	3.79	3.14	564.04	24.09	0.31	1182	8.12	2120
7	1692.45	23.395	172.461	9.322	3.60	3.37	608.05	5.93	0.47	1232	8.29	2230
8	1555.49	81.232	57.896	8.195	2.65	0.58	562.05	2.52	0.15	1058	7.94	2020
9	1007.64	52.185	58.902	5.756	3.49	0.70	347.50	3.26	0.70	754	8.13	1524
10	1702.23	1.617	75.026	6.400	3.84	0.88	562.20	2.09	0.39	1096	8.29	2020
Average	1415.59	82.80	180.01	7.32	11.18	5.22	554.42	16.76	0.66	1182.50	8.12	2183.60
Coefficient of variation	0.18	2.24	0.64	0.24	1.76	1.71	0.14	1.17	1.02	0.17	0.02	0.16

The coefficient of variation is the ratio of the standard deviation to the average, and it reflects the degree of dispersion on the unit average value. Its calculation formula is as follows:

$$\gamma = s/x_m, \tag{1}$$

$$s = \sqrt{\frac{1}{n-1}\sum_{i=1}^{n}(x_i - x_m)^2}, \tag{2}$$

where γ is the coefficient of variation, s is the standard deviation, x_m is the average value, n is the total number of samples, and x_i is the measured value of an individual sample.

SO$_4$ had a higher coefficient of variation than the other ions, which shows that its change was more significant. Ions with a coefficient of variation over 1 included SO$_4$, Ca, Mg, and K. A larger coefficient of variation shows that an ion has greater instability within the chemical composition of the water, and it indicates a more complex groundwater composition formation process [27].

The ratios of the average values o" the ion concentrations in each coal seam reflect the differences between the water chemistry of the coal seams. The ratios for No. 15 coal seam to those of No. 3 coal seam showed that the produced water of No. 15 coal seam was significantly enriched in SO$_4$ and relatively enriched in Ca and Mg. Additionally, the coefficient of variation of ions in the water produced by No. 15 coal seam was larger than that of No. 3 coal seam, which indicated that the water in No. 15 coal seam had undergone a more complex water chemical formation process. The coefficients of variation of SO4, Ca, and Mg were greater than 1 for No. 15 coal seam, and these evidently underwent more significant changes than the other ions. The coefficient of variation of the ions in No. 3 coal seam were all less than 1 (Table 2).

Table 2. Statistics of ionic compositions in produced water samples of No. 3 and No. 15 coal seams.

Samples	Coal Seam Number	HCO$_3^-$ (mg/L)	SO$_4^{2-}$ (mg/L)	Cl$^-$ (mg/L)	F$^-$ (mg/L)	Ca^{2+} (mg/L)	Mg^{2+} (mg/L)	Na$^+$ (mg/L)	K$^+$ (mg/L)	Sr^{2+} (mg/L)	TDS (mg/L)	pH	EC (μS/cm)
	3	1467.45	1.49	240.53	6.33	4.58	0.98	584.24	20.30	0.42	1232	8.16	2306.00
Average	15	1354.94	167.99	250.90	8.22	21.01	10.92	586.08	27.33	1.00	1333.50	8.05	2417.50
	15/3	0.92	112.97	1.04	1.30	4.59	11.14	1.00	1.35	2.40	1.08	0.99	1.05
Coefficient of variation	3	0.01	0.84	0.53	0.19	0.17	0.55	0.08	0.77	0.35	0.13	0.00	0.11
	15	0.22	1.61	0.35	0.26	1.34	1.10	0.05	0.87	0.94	0.10	0.03	0.10

The water can be classified into four types using the Piper diagram: Ca-(SO$_4$)-Cl, Ca-HCO$_3$, Na-(SO$_4$)-Cl, and Na-HCO$_3$ [27]. As shown in Figure 2, the produced water sample types were mainly Na-HCO$_3$, except for sample No. 5, which was Na-(SO4)-Cl. Therefore, all the produced water samples were of an Na-type. Sample No. 5 contained higher concentrations of SO$_4$, Ca, Mg, and TDS than the other samples but comparatively lower concentrations of HCO$_3$. Samples from the MCWs (No. 8, 9, and 10) were relatively HCO3-rich and Cl-poor compared to the SPW samples.
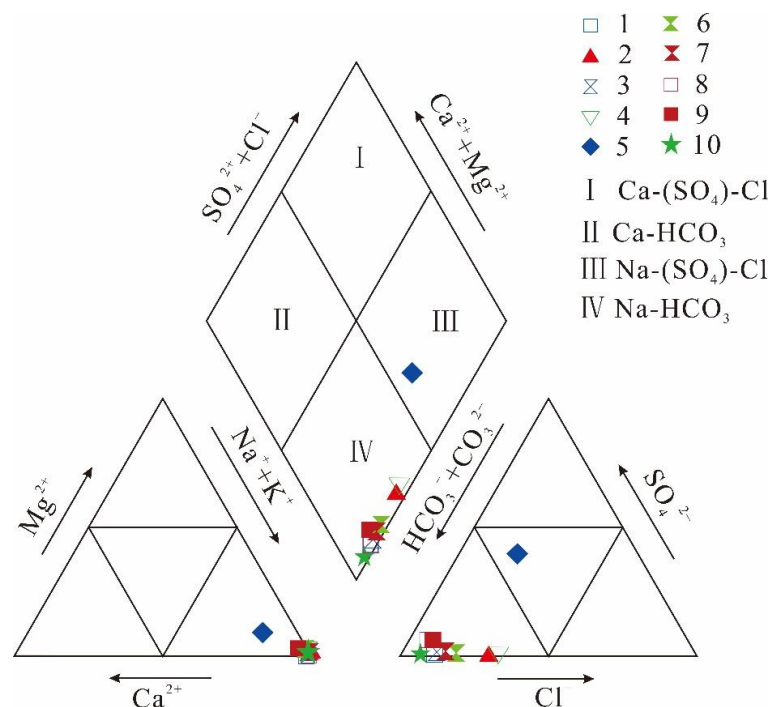

Figure 2. Piper diagram of the ionic compositions of produced water samples.

The differences in the ionic compositions reflect the different depositional environments of the two coal seams (Nos. 3 and 15). Under the sedimentary background of the late Paleozoic sea–land transitional facies in the study area, the Shanxi Formation was dominated by shallow water deltas with relatively developed distributary channels, while the Taiyuan Formation was dominated by lagoons/tidal flats, with carbonate-bearing tidal flat deposits and multiple sets of developed biological debris limestone. Therefore, No. 15 coal seam, which was more strongly affected by seawater during its deposition, was found to have a higher sulfur content, and this caused the produced water to have a higher SO_4 concentration than that of No. 3. The water produced by No. 15 coal seam also had high Ca and Mg concentrations, which may be related to the dissolution of carbonate minerals in the coal seam and its limestone roof.

4.2. Relationships between the Major Ions of the Produced Water Samples

A correlation analysis between different ions was used to analyze the geochemical characteristics and primary controlling factors of the water produced from the CBM wells. To examine the differences between the water produced from co-production wells and single-SPWs, the data from single-SPWs were fitted, and the 95% confidence interval of the fitting equation was determined. As shown in Figure 3a, all the samples are located at a distance from the 1:1 line of Cl^- versus Na^+, showing that halite dissolution was not the primary source of Cl^- and Na^+ in water and that the relative enrichment of Na^+ was caused by other factors. The location of the MCWs was outside the 95% confidence interval of the fitting line for SPWs, and this reflects the differences between the water produced from MCWs and SPWs. Additionally, sample 7 from an SPW was outside the confidence interval. The fact that Well 7 is vertical and the other SPWs are horizontal illustrates the difference between the two well types. Generally, MCWs are straight wells with a large span, which means that their water sources communicate with other water sources during drainage, and this produces the different ionic composition characteristics. For SPWs, it is easier for vertical wells to communicate with neighboring aquifers than horizontal wells, and the water produced from horizontal wells thus better reflects the characteristics of the in situ coal seam water.
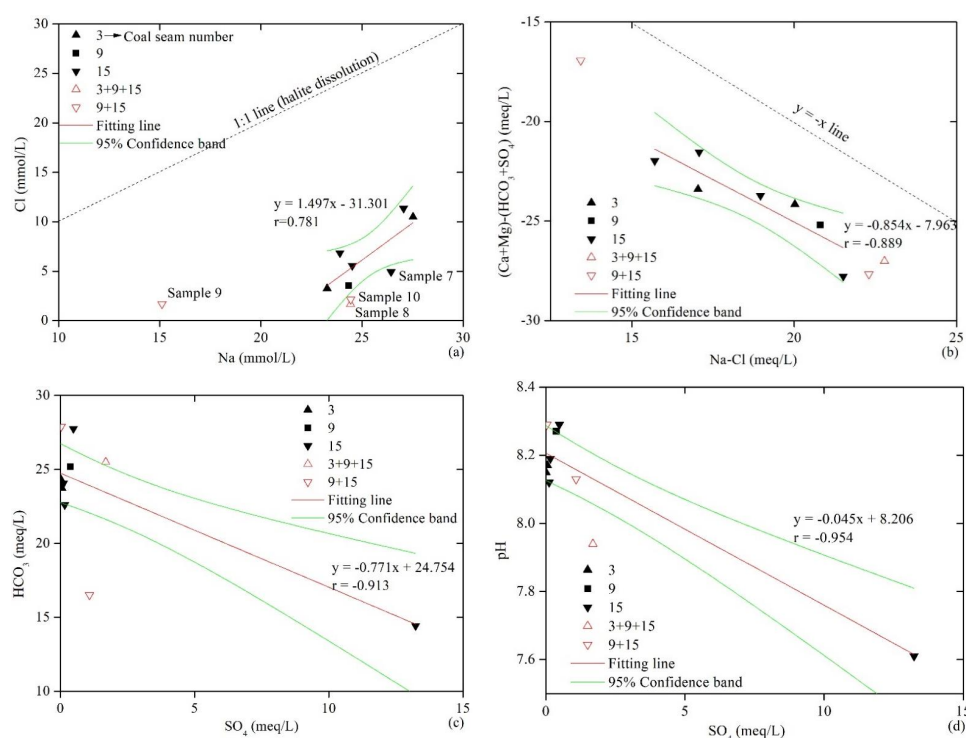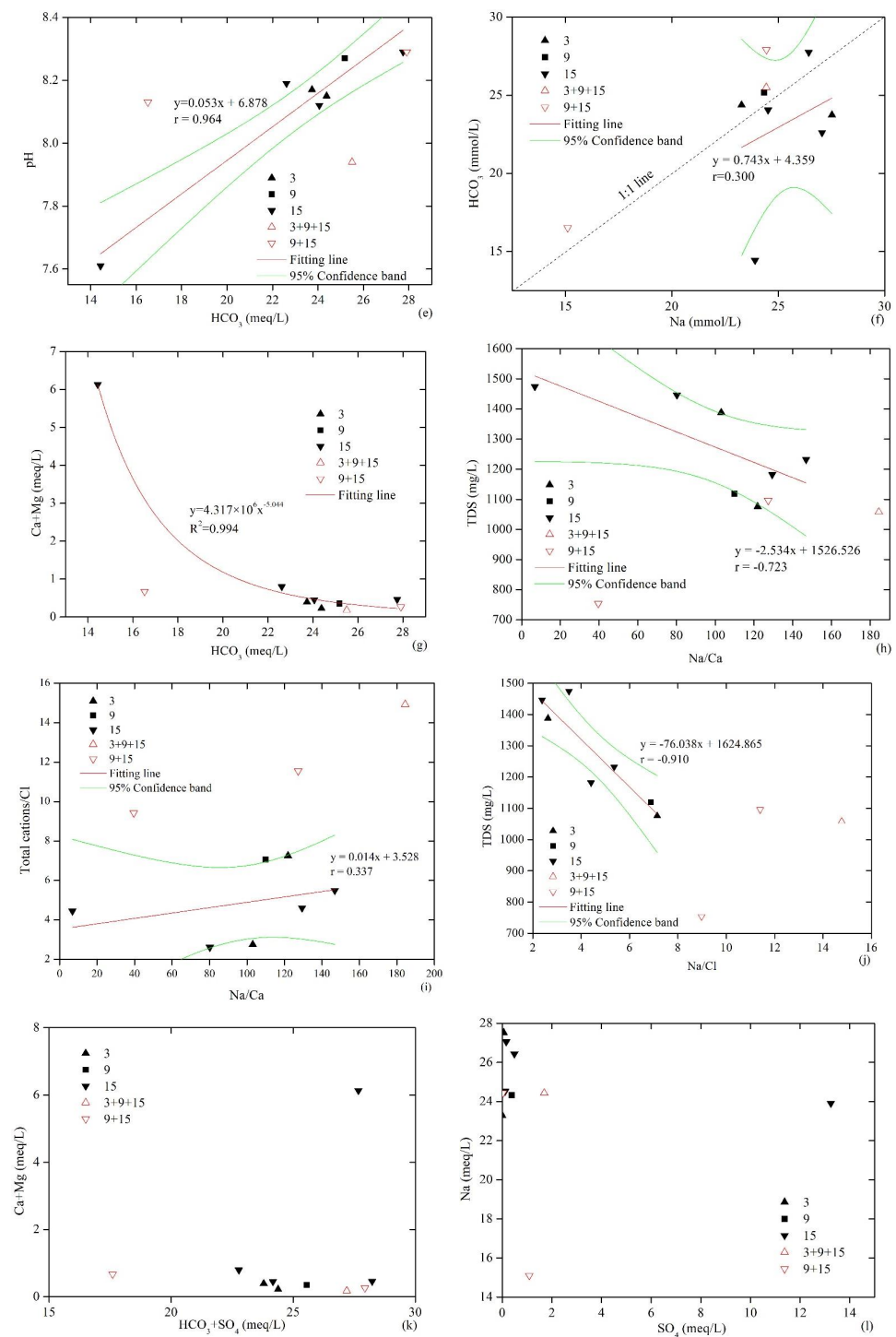

Figure 3. *Cont.*

Figure 3. Relationships between the ionic compositions of produced water samples. (**a**) Na versus Cl; (**b**) Na − Cl versus (Ca + Mg) − (HCO_3 + SO_4); (**c**) SO_4 versus HCO_3; (**d**) SO_4 versus pH; (**e**) HCO_3 versus pH; (**f**) Na versus HCO_3; (**g**) HCO_3 versus Ca + Mg; (**h**) Na/Ca versus TDS; (**i**) Na/Ca versus Total cations/Cl; (**j**) Na/Cl versus TDS; (**k**) HCO_3 + SO_4 versus Ca + Mg; (**l**) SO_4 versus Na.

Cation exchange adsorption is one of the key factors involved in the enrichment of Na^+ in the groundwater of coal measures, and the relationship between (Na^+ − Cl^-) versus (Ca^{2+} + Mg^{2+}) − (HCO_3^- + SO_4^{2-}) provides information about this. If there is a linear relationship between the two and the slope is close to −1, cation exchange adsorption is considered to have a prevailing influence on groundwater. A linear fit to the SPW data showed the slope of the fitted line was −0.854 and the correlation coefficient was −0.889,

which indicated the important impact of cation exchange adsorption on the produced water quality and the contribution to the source of Na^+ Figure 3b. The MCW data differed from those of SPW, and they also represented the recharging effect during commingled production. However, the data of MCW followed a linear relationship, which indicated the control of cation exchange on the produced water. Further investigation revealed that all data points were below the line of $y = -x$, which indicated that Ca^{2+} and Mg^{2+} were consumed at a higher level than the amount of Na^+ produced. The consumption of Ca^{2+} and Mg^{2+} in groundwater relates to factors other than cation exchange adsorption, such as the precipitation of carbonate and sulfate minerals.

Sulfate reduction is a characteristic water–rock interaction in the groundwater of coal measures. In a reduced environment with the presence of SO_4^{2-} reducing bacteria, SO_4^{2-} tends to be reduced to H_2S, and the organic carbon components (including methane) in coals tend to be oxidized to HCO_3^-. This process promotes the increase in pH and the precipitation of Ca^{2+} and Mg^{2+}. The chemical reaction formula is as follows:

$$SO_4^{2-} + 2C \text{ (organic matter)} + 2H_2O \rightarrow H_2S + 2HCO_3^-, \tag{3}$$

$$CH_4 + SO_4^{2-} + H^+ \rightarrow H_2O + H_2S + HCO_3^-, \tag{4}$$

$$HCO_3^- + H_2O \rightarrow H_2CO_3 + OH^-, \tag{5}$$

$$Ca^{2+} (Mg^{2+}) + 2HCO_3^- \rightarrow Ca(Mg)CO_3 + CO_2 + H_2O. \tag{6}$$
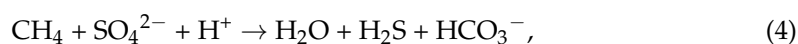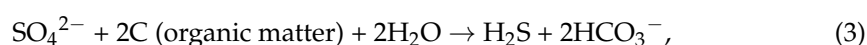
Figure 3c shows that SO_4^{2-} and HCO_3^- were negatively correlated, and Figure 3d and d show that the pH value was negatively correlated with SO_4^{2-} and positively correlated with HCO_3^-; this provides evidence of sulfate reduction in groundwater. As shown in Figure 3f, the correlation between HCO_3^- and Na^+ was not obvious, and this reflected their different sources. Data from the MCWs and SPWs of No. 3 and 9 coal seams were mostly located above the 1:1 line ($HCO_3^- > Na^+$), and data from the SPWs of No. 15 coal seam were mostly located below the line ($HCO_3^- < Na^+$). The primary sources of HCO_3^- in groundwater mainly include atmospheric precipitation recharge, sulfate reduction, mineral dissolution and weathering, and organic matter fermentation. Figure 3g shows that there was no positive correlation between HCO_3^- and ($Ca^{2+}+Mg^{2+}$), indicating that the dissolution of carbonate minerals was not the main cause of HCO_3^- enrichment. Weathering of silicate minerals causes a positive correlation between HCO_3^- and Na, and the ratio of HCO_3^- to Na^+ is slightly greater than 2:1. HCO_3^- and Na do not fit this relationship here, and this proves that silicate weathering is not the primary source of HCO_3^-. Acetic acid fermentation leads to formation of CO_2, which dissolves in water to generate HCO_3^- [28,29] as follows:

$$CH_3COOH \rightarrow CO_2 + CH_4, \tag{7}$$

$$CO_2 + H_2O \rightleftharpoons HCO_3^- + H^+. \tag{8}$$

However, the above reaction is very limited for high-rank coals, and the extremely low content of CO_2 in CBM provides such evidence. Therefore, it can be considered that the abundant HCO_3^- in the produced water was mainly derived from the original composition of the recharge water and sulfate reduction. The atmospheric precipitation and surface water quality in this area are mainly of an HCO_3^--Ca^{2+} type. The production layer of the CBM wells is generally shallow, and the drainage tends to be affected by shallow groundwater [3]. Data of the co-production wells were located above the 1:1 line of HCO_3^- versus Na^+, which shows that recharge contributed to the excess HCO_3^-. In contrast, the water produced by No. 15 coal seam was relatively rich in Na.

As shown in Figure 3h,i, Na^+/Ca^{2+} correlated negatively with TDS and had a positive correlation with total cations/Cl^-, which indicates that, in addition to cation exchange adsorption, the high TDS water was formed via other geochemical processes. There was a significant negative correlation between Na^+/Cl^- and TDS (Figure 3j; this indicated

that the formation of high TDS water was characterized by an increase in Cl^- that was the result of the gradual enrichment of soluble Cl^- under retention conditions. Additionally, the data distribution of MCW is discrete and different from that of SPW in the relationships of Na^+/Cl^- versus TDS and Na^+/Ca^{2+} versus total cations/Cl^-, and this reflects their obviously different water sources. It can thus be concluded that the water sources of MCWs communicate outside the coal seams with low Cl^-, and this provides the typical characteristics.

Figure 3k shows that there was no clear correlation between ($HCO_3^- + SO_4^{2-}$) and ($Ca^{2+} + Mg^{2+}$), and Ca^{2+} and Mg^{2+} were severely depleted compared with HCO_3^- and SO_4^{2-}; this indicates that the dissolution of gypsum and carbonate minerals was not dominant in groundwater, and the excess HCO_3^- and SO_4^{2-} could only be neutralized by the Na^+ in the produced water. Furthermore, there was no discernible relationship between SO_4^{2-} and Na^+ (Figure 3l), indicating that the dissolution of mirabilite ($Na_2SO_4 \cdot 10H_2O$) was not the primary source of SO_4^{2-}. The source of SO_4^{2-} in the produced water should mainly relate to the original composition of recharge water and pyrite oxidation. However, considering that No. 15 coal seam is more enriched in SO_4^{2-} than No. 3 coal seam, this difference cannot be explained only by the original recharge water composition. The relative enrichment of SO_4^{2-} in the produced water from No. 15 coal seam should be related to the oxidation and dissolution of pyrite, which is the main carrier of sulfur in high-sulfur coals, where the oxidation reaction of pyrite is as follows:

$$4FeS_2 + 15O_2 + 14H_2O \rightarrow 4Fe(OH)_3 + 8SO_4^{2-} + 16H^+. \tag{9}$$
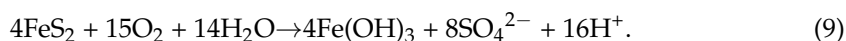
The roof of the No. 15 coal seam is a limestone layer termed "K_2," and it constitutes a relatively strong hydrodynamic system. The groundwater flow brings O_2 into coals, which leads to the oxidation and dissolution of pyrite and the enriched SO_4^{2-} in the produced water. Mining activities also aggravate this reaction. Sample 5 is the most typical of pyrite oxidation, and it has the highest SO_4^{2-} concentration and the lowest pH value.

4.3. Principal Component Analysis

Principal component analysis is widely used in hydrochemistry analysis. By reducing the data dimensions, it reorganizes several interrelated variables and forms independent new variables, which can effectively reduce data redundancy and assist in discovering key information that is hidden in high-dimensional data. In this study, the ionic concentration data of the produced water were analyzed using principal component analysis. Two principal components (PC1 and PC2) with eigenvalues >1 were extracted, and the variance contribution rates were found to be 50.22% and 30.00%, respectively. The cumulative variance contribution rate was 80.22%, indicating that the two components could describe most of the information in the data (Table 3). The correlation coefficients for each component and ions are shown in Table 4. The correlation coefficient between an ion and the principal component is termed the load value of an ion on the principle component. The characteristic ions in each principal component were extracted with a correlation coefficient of >0.6 as the standard. PC1 had a significant positive correlation with SO_4^{2-}, Ca^{2+}, and Mg^{2+}. These ions were relatively enriched in the produced water of No. 15 coal seam and were related to pyrite oxidation and carbonate mineral dissolution. PC1 showed an obvious negative correlation with HCO_3^- and F^-, which reflected the oxidation of pyrite to produce H^+, resulting in the loss of HCO_3^-. The reverse reaction of pyrite oxidation represented by PC1 was sulfate reduction, which related to a decrease in SO_4^{2-}, an increase in HCO_3^- and pH, and the precipitation of Ca and Mg. Additionally, sulfate reduction resulted in increased pH, which promoted ion exchange between F^--OH^- and led to an increased F^- concentration. Previous studies have also pointed out that the alkaline water environment is conducive for enrichment of F^- [30]. The F^- concentration (average 7.32 mg/L) of the produced water samples far exceeded the drinking water standard (1 mg/L), and this should be considered during later treatment plans. PC2 showed a significant positive correlation with Cl^-, Na^+, and K^+, which reflected the characteristics of gradually enriching

soluble ions via the enhanced water–rock interactions and groundwater retention degree (Figure 4).

Table 3. Eigenvalues of each principal component.

Principal Component	Initial Eigenvalues		
	Total	**% of Variance**	**Cumulative %**
PC1	4.017	50.22	50.22
PC2	2.400	30.00	80.22

Table 4. Correlation coefficient for each principal component.

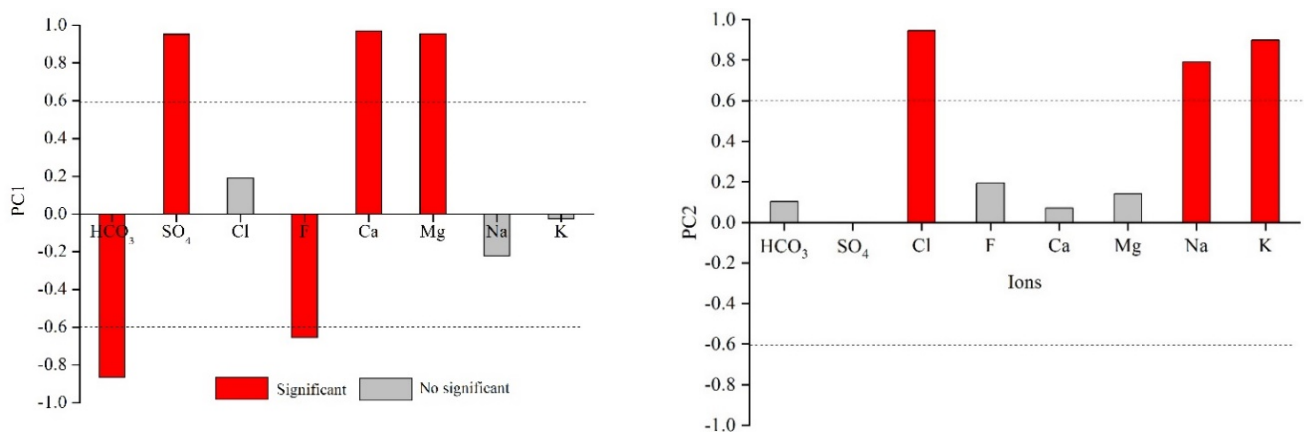| Ions	Principal Component	
	1	**2**
HCO_3	−0.865	0.103
SO_4	0.952	−0.005
Cl	0.189	0.945
F	−0.655	0.194
Ca	0.969	0.071
Mg	0.953	0.142
Na	−0.223	0.791
K	−0.023	0.899

Figure 4. Extraction of characteristic ions from principal components.

The load value distribution of each ion on the principal components, PC1 and PC2, was further obtained using the varimax-rotation method [31]. As shown in Figure 5, the load values of SO_4^{2-}, Ca^{2+}, and Mg^{2+} on PC1 are highly positive, while those of $HCO3^-$ and F^- are highly negative, and these are distributed along the PC1 axis. Therefore, PC1 reflects the oxidation of pyrite and the dissolution of carbonate and sulfate minerals, and its opposite represents sulfate reduction and the promotion of Ca and Mg precipitation. The load values of Cl^+, K^+, and Na^+ on PC2 are highly positive, thereby reflecting the characteristic water–rock interactions of the coal measure, such as cation exchange adsorption. A higher value reflects that the groundwater is increasingly stagnant. The opposite of PC2 represents an active groundwater type or strong recharge conditions. PC2 can be used to distinguish the water produced in MCWs from that of SPWs, which have lower Cl^-, Na^+, and K^+ concentrations due to the active external water supply. Recharge plays a significant role in the water quality variations, and, with an increasing distance from the recharge area or a reduced flow capacity, there were increases and decreases in the Cl and Na and Ca and Mg concentrations, respectively [4]. Almost all the ions are located above the PC2 zero line and within the first and second quadrants of Figure 5, which reflects the overall strong

water–rock interactions and stagnant groundwater conditions that exert varying degrees of promoting effects on the ion concentrations.
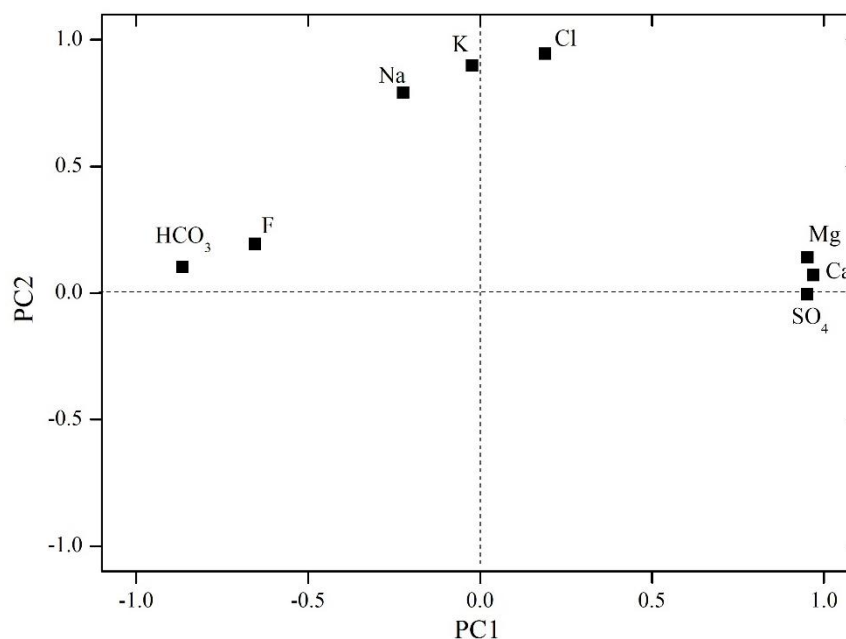

Figure 5. Distribution of ion load values on principal components.

The ionic concentration data from 10 water samples were multiplied by the load values on each principal component to obtain the load score of each sample on each principal component. The specific calculation formulas used were as follows:

$$S_{PC1} = -0.865HCO_3 + 0.952SO_4 + 0.189Cl - 0.655F + 0.969Ca + 0.953Mg - 0.223Na - 0.023K \tag{10}$$

$$S_{PC2} = 0.103HCO_3 - 0.005SO_4 + 0.954Cl + 0.194F + 0.071Ca + 0.142Mg + 0.791Na + 0.899K \tag{11}$$

where S_{PC1} and S_{PC2} are the load scores of each sample on PC1 and PC2, respectively, and ions in the formulas are presented at the milligram equivalent concentration (meq/L). The relationship between each sample and the principal component was analyzed by drawing a scatterplot between S_{PC1} and S_{PC2}, and Figure 6 shows that the samples are mainly located in the second quadrant, which implies that the ionic composition of the produced water is mainly related to the strong water–rock interactions of the coal measure. The stagnant degree of the groundwater is high, and sulfate reduction is stronger than pyrite oxidation. Only sample 5 from coal seam No. 15 is located in the first quadrant, which is representative of the strongest pyrite oxidation and carbonate dissolution processes. Additionally, the water samples from MCWs are all located in a lower position than those of SPWs, which reflect their relatively open hydrochemical characteristics caused by recharge from active external water.

4.4. Geochemical Formation Model of Produced Water

The geochemical formation model of water produced from CBM wells in this area can be summarized as follows: after the coal seam (coal measure) is recharged by the atmospheric precipitation or surface water, the water quality type is mainly Ca-HCO$_3$ or Ca-(SO$_4$)-HCO$_3$. In the process of groundwater runoff to depths and mineral dissolution from carbonate, sulfate, and salt rocks, the chemical composition of the water is transformed; however, due to the strong recharge in the shallow strata, there is little change to the water quality. With an increase in depth, the reducibility gradually increased, and cation exchange adsorption and sulfate reduction gradually become the main water–rock interactions of the coal measure, and this is reflected in the loss of Ca, Mg, SO$_4$, and the increase in Na, HCO$_3$,

and pH. Additionally, soluble Cl and TDS increase synchronously with the enhanced water–rock interactions. On this basis, the produced water of No. 15 coal seam in Taiyuan Formation, which was formed in a marine background, undergoes pyrite oxidation, which results in a higher SO_4 content and lower pH. As a result, dissolution of the carbonate and sulfate minerals in the coal seam and its limestone roof are accelerated, which results in higher Ca and Mg concentrations in the produced water than those of No. 3 coal seam. The ionic compositions of MCW do not lie between those of the coal seams of SPWs, but they are discretely distributed, which implies that the external water is recharged during multi-seam co-production [32], and it is characterized by low Cl and TDS values Figure 7. The production of external water inhibits reservoir depressurization and causes a lower gas production efficiency, which explains the main reasons for the low productivity of the CBM commingled wells in the Shanxi and Taiyuan Formations in this area.
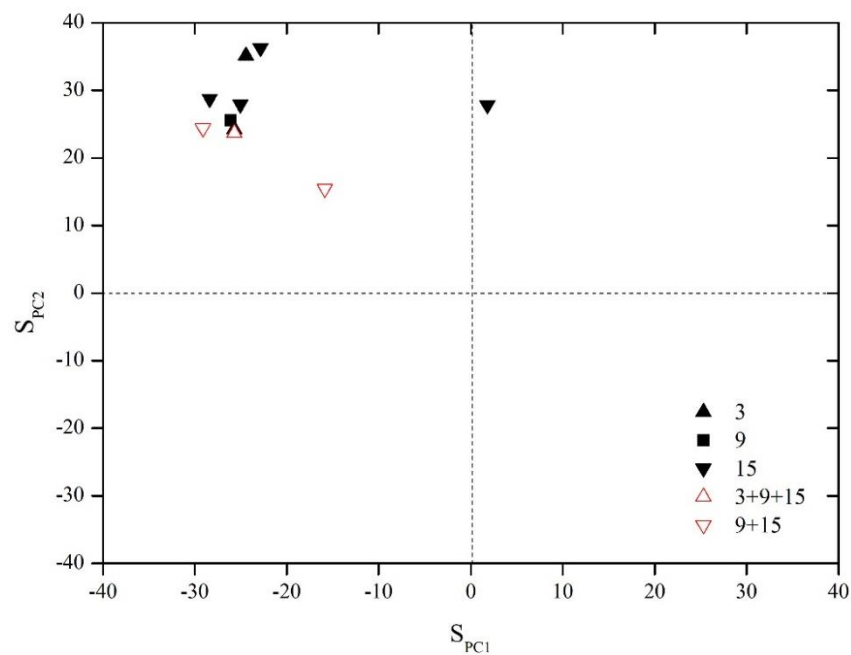

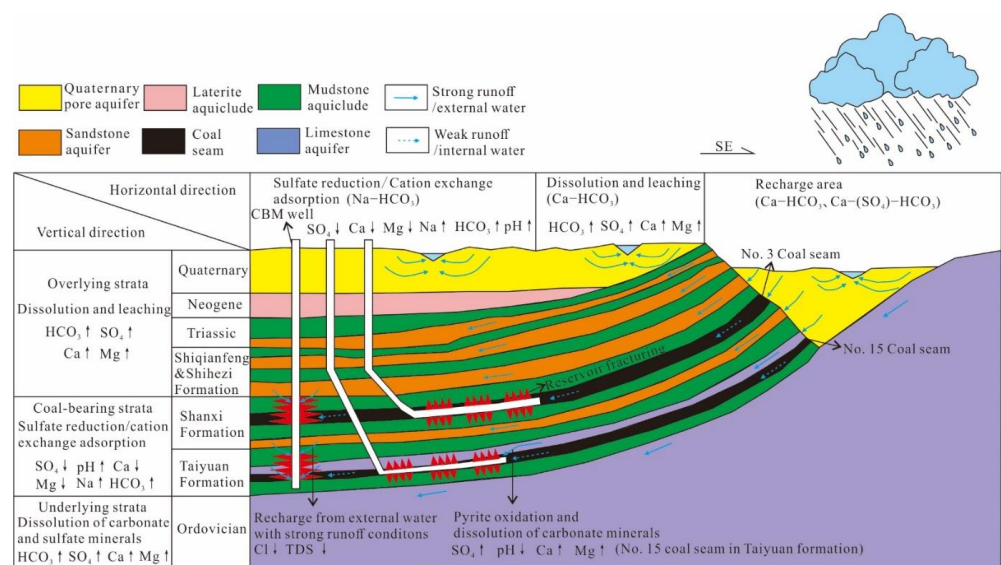**Figure 6.** Load scores of produced water samples on principle components.

Figure 7. Model of the geochemical formation of produced water.

5. Conclusions

(1) Na-HCO$_3$-type water is the predominant produced water type in samples collected from the CBM wells in the southern Qinshui Basin. The water produced from No. 15 coal seam is comparatively more enriched in SO$_4$ and relatively enriched in Ca and Mg than that from No. 3 coal seam. The coefficients of variation of the above three ions in No. 15 coal seam are all greater than 1, while the coefficients of variation of each ion in No. 3 coal seam are all less than 1, which shows that the chemical formation process of produced water from No. 15 coal seam is more complex than that of No. 3 coal seam. The water type of sample 5 from No. 15 coal seam differs from the other water samples in that it is Na-(SO$_4$)-Cl, its SO$_4$ concentration is significantly higher than that of the other samples, and it contains higher levels of Ca, Mg, and TDS and lower levels of HCO$_3$.

(2) Based on the correlation analysis and principal component analysis of the ionic composition characteristics, two characteristic components were extracted, and these represent two hydrochemical formation process types. The first type represents pyrite oxidation and carbonate and sulfate dissolution, and its opposite represents sulfate reduction. The second type reflects groundwater retention and confinement characteristics, and its opposite represents an active groundwater type or stronger recharge conditions. We thus used this information to construct a geochemical formation model of the water produced from the CBM wells in the study area. This showed that cation exchange adsorption and sulfate reduction are the main water–rock interactions occurring in the coal measure, and pyrite oxidation exists in the produced water from No. 15 coal seam of the Taiyuan Formation, which further contributes to the accelerated dissolution of carbonate minerals in the limestone roof of No. 15 coal seam.

(3) The ionic data for the water produced from the MCWs do not follow the rules of those for the coal seams of the SPW, nor do they satisfy the linear relationship between the ionic compositions of the SPW, which show that the MCWs and SPWs have different water sources. The ionic compositions of the water produced from the MCWs are characterized by low Cl and TDS. The MCWs receive recharge from external water sources during the drainage process, which limits the efficiency of the reservoir pressure drop, and this is the main reason for the poor CBM co-production effect from the Shanxi and Taiyuan Formations in this area.

Author Contributions: Conceptualization, J.W. and C.G.; methodology, J.W.; software, C.G.; validation, S.S.; formal analysis, G.L.; investigation, J.W. and C.G.; resources, G.L.; data curation, S.S.; writing—original draft preparation, J.W.; writing—review and editing, C.G.; visualization, S.S.; supervision, G.L.; project administration, G.L.; funding acquisition, J.W. and C.G. All authors have read and agreed to the published version of the manuscript.

Conflicts of Interest: The authors declare no conflict of interest.

References

1. Rice, C.A. Production waters associated with the Ferron coalbed methane fields, central Utah: Chemical and isotopic composition and volumes. *Int. J. Coal Geol.* **2003**, *56*, 141–169. [CrossRef]
2. Rice, C.A.; Flores, R.M.; Stricker, G.D.; Ellis, M.S. Chemical and stable isotopic evidence for water/rock interaction and biogenic origin of coalbed methane, Fort Union Formation, Powder River Basin, Wyoming and Montana U.S.A. *Int. J. Coal Geol.* **2008**, *76*, 76–85. [CrossRef]

3. Guo, C.; Qin, Y.; Xia, Y.C.; Ma, D.M.; Han, D.; Chen, Y.; Chen, W.; Jian, K.; Lu, L.L. Geochemical characteristics of water produced from CBM wells and implications for commingling CBM production: A case study of the Bide-Santang Basin, western Guizhou, China. *J. Pet. Sci. Eng.* **2017**, *159*, 666–678. [CrossRef]

4. Guo, C.; Qin, Y.; Han, D. Interlayer interference analysis based on trace elements in water produced from coalbed methane wells: A case study of the upper Permian coal-bearing strata, Bide-Santang basin, western Guizhou, China. *Arab. J. Geosci.* **2017**, *10*, 137. [CrossRef]

5. Klein, D.A.; Flores, R.M.; Venot, C.; Gabbert, K.; Schmidt, R.; Stricker, G.D.; Pruden, A.; Mandernack, K. Molecular sequences derived from Paleocene fort union formation coals vs. associated produced waters: Implications for CBM regeneration. *Int. J. Coal Geol.* **2008**, *76*, 3–13. [CrossRef]

6. Baublys, K.A.; Hamilton, S.K.; Golding, S.D.; Vink, S.; Esterle, J. Microbial controls on the origin and evolution of coal seam gases and production waters of the Walloon Subgroup; Surat Basin, Australia. *Int. J. Coal Geol.* **2015**, *147–148*, 85–104. [CrossRef]

7. Qin, Y.; Zhang, Z.; Bai, J.; Liu, D.; Tian, Y. Source apportionment of produced water and feasibility discrimination of com-mingling CBM production from wells in southern Qinshui basin. *J. China Coal Soc.* **2014**, *39*, 1892–1898.

8. Snyder, G.T.; Riese, W.C.; Franks, S.; Fehn, U.; Pelzmann, W.L.; Gorody, A.W.; Moran, J.E. Origin and history of waters associated with coalbed methane: 129I, 36Cl, and stable isotope results from the Fruitland formation, CO and NM. *Geochim. Cosmochim. Acta* **2003**, *67*, 4529–4544. [CrossRef]

9. Snyder, G.T.; Fabryka-Martin, J.T. 129I and 36Cl in dilute hydrocarbon waters: Marine cosmogenic, in situ, and anthropogenic sources. *Appl. Geochem.* **2007**, *22*, 692–714. [CrossRef]

10. Yang, Z.B.; Qin, Y.; Qin, Z.H.; Yi, T.S.; Li, C.L.; Zhang, Z.G. Dissolved inorganic carbon in water produced from coalbed wells and its geological significance. *Pet. Explor. Dev.* **2020**, *47*, 202081. [CrossRef]

11. Ma, X.; Song, Y.; Liu, S.; Jiang, L.; Hong, F. Origin and evolution of waters in the Hancheng coal seams, the ordos basin, as revealed from water chemistry and isotope (H, O, 129I) analyses. *Sci. China Earth Sci.* **2013**, *56*, 1962–1970. [CrossRef]

12. Cheung, K.; Sanei, H.; Klassen, P.; Mayer, B.; Goodarzi, F. Produced fluids and shallow groundwater in coalbed methane (CBM) producing regions of Alberta, Canada: Trace element and rare earth element geochemistry. *Int. J. Coal Geol.* **2009**, *77*, 338–349. [CrossRef]

13. Dahm, K.G.; Guerra, K.L.; Xu, P.; Drewes, J.E. Composite geochemical database for coalbed methane produced water quality in the rocky mountain region. *Environ. Sci. Technol.* **2011**, *45*, 7655–7663. [CrossRef] [PubMed]

14. Dahm, K.G.; Guerra, K.L.; Munakata-Marr, J.; Drewes, J.E. Trends in water quality variability for coalbed methane produced water. *J. Clean. Prod.* **2014**, *84*, 840–848. [CrossRef]

15. Qin, Y.; Wu, J.G.; Li, G.Z.; Wang, Y.B.; Shen, J.; Zhang, B.; Shen, Y.L. Patterns and pilot project demonstration of coal measures gas production. *J. China Coal Soc.* **2020**, *45*, 2513–2522.

16. Guo, C.; Qin, Y.; Wu, C.F.; Lu, L.L. Hydrogeological control and productivity modes of coalbed methane commingled pro-duction in multi-seam areas: A case study of the Bide-Santang Basin, western Guizhou, South China. *J. Petrol. Sci. Eng.* **2020**, *189*, 107039. [CrossRef]

17. Guo, C.; Qin, Y.; Sun, X.Y.; Wang, S.Q.; Xia, Y.C.; Ma, D.M.; Bian, H.Y.; Shi, Q.M.; Chen, Y.; Bao, Y.; et al. Physical simulation and compatibility evaluation of multi-seam CBM co-production: Implications for the development of stacked CBM systems. *J. Petrol. Sci. Eng.* **2021**, *204*, 108702. [CrossRef]

18. Guo, C.; Gao, J.Z.; Wang, S.Q.; Zhang, C.; Li, X.; Gou, J.; Lu, L.L. Groundwater geochemical variation and controls in coal seams and overlying strata in the Shennan mining area, Shaanxi, China. *Mine Water Environ.* **2022**, *41*, 614–628. [CrossRef]

19. Ripepi, N.; Louk, K.; Amante, J.; Schlosser, C.; Tang, X.; Gilliland, E. Determining coalbed methane production and composition from individual stacked coal seams in a multi-zone completed gas well. *Energies* **2017**, *10*, 1533. [CrossRef]

20. Pashin, J.C. Variable gas saturation in coalbed methane reservoirs of the Black Warrior Basin: Implications for exploration and production. *Int. J. Coal Geol.* **2010**, *82*, 135–146. [CrossRef]

21. Nelson, P.H. Pore-throat sizes in sandstones, tight sandstones, and shales. *AAPG Bull.* **2009**, *93*, 329–340. [CrossRef]

22. Ju, Y.W.; Wei, M.M.; Hou, Q.L.; Wang, G.L.; Xue, C.D. The tectonic differentiation of the coal basins and the emplacement models of the deep coal in north China. *J. China Coal Soc.* **2010**, *35*, 1501–1505.

23. Liu, H.J.; Qin, Y.; Sang, S.X. *Geology of Coal-Bed Methane in Southern Shanxi*; China University of Mining and Technology Press: Xuzhou, China, 1998; pp. 1–151.

24. Zhang, Z.; Qin, Y.; Bai, J.; Li, G.; Zhuang, X.; Wang, X. Hydrogeochemistry characteristics of produced waters from CBM wells in Southern Qinshui basin and implications for CBM commingled development. *J. Nat. Gas Sci. Eng.* **2018**, *56*, 428–443. [CrossRef]

25. Qin, Y.; Gao, D.; Wu, C.F.; Yi, T.S.; Hong, Y.J. *Coalbed Methane Resources Potential and Evaluation of Guizhou Province*; China University of Mining and Technology Press: Xuzhou, China, 2012; pp. 12–18.

26. Meng, Q.C.; Zhang, Y.P.; Guo, X.B.; Sun, Y.J.; Zhang, J.J. Evaluation of high-grade coal-bed methane in the southern part of Qinshui Basin and its effectiveness: A case study of Zhengzhuang-Fanzhuang block. *Nat. Gas Ind.* **2011**, *31*, 14–17+118–119.

27. Chae, G.-T.; Yun, S.-T.; Mayer, B.; Kim, K.-H.; Kim, S.-Y.; Kwon, J.-S.; Koh, Y.-K. Fluorine geochemistry in bedrock groundwater of South Korea. *Sci. Total Environ.* **2007**, *385*, 272–283. [CrossRef]

28. Whiticar, M.J. Carbon and hydrogen isotope systematics of bacterial formationand oxidation of methane. *Chem. Geol.* **1999**, *161*, 291–314. [CrossRef]

29. Flores, R.M. *Coal and Coalbed Gas: Fueling the Future*; Elsevier Inc. Press: Cambridge, MA, USA, 2014.

30. Zhang, Z.; Li, G.Q.; Su, X.B.; Zhuang, X.G.; Wang, L.; Fu, H.J.; Li, L. Geochemical controls on the enrichment of fluoride in the minewater of the Shendong mining area. *China Chemos.* **2021**, *284*, 131388. [CrossRef]
31. Chen, L.W.; Xu, D.Q.; Yin, X.X.; Xie, W.P.; Zeng, W. Analysis on hydrochemistry and its control factors in the concealed coal mining area in north China: A case study of dominant inrush aquifers in Suxian mining area. *J. China Coal Soc.* **2017**, *42*, 996–1004.
32. Guo, C.; Qin, Y.; Yi, T.S.; Chen, Z.L.; Yuan, H.; Gao, J.Z.; Gou, J. A method for identifying coalbed methane co-production interference based on production characteristic curves: A case study of the Zhijin block, western Guizhou, China. *Pet. Explor. Dev.* **2022**, *49*, 977–986.